UNIVERSIDADE FEDERAL DE ITAJUBÁ
INSTITUTO DE RECURSOS NATURAIS
PROGRAMA DE GRADUAÇÃO EM CIÊNCIAS ATMOSFÉRICAS

THE WIND ENERGY RESOURCE OF A LARGE TROPICAL AQUATIC SYSTEM: HIGH RESOLUTION NUMERICAL ASSESSMENT AND THE ATMOSPHERIC STABILITY EFFECTS TO POWER PRODUCTION

BSc MONOGRAPH

Bruno de Campos

Itajubá, MG, Brazil

2015

THE WIND ENERGY RESOURCE OF A LARGE TROPICAL AQUATIC SYSTEM: HIGH RESOLUTION NUMERICAL ASSESSMENT AND THE ATMOSPHERIC STABILITY EFFECTS TO POWER PRODUCTION

by

Bruno de Campos

Dissertation presented to the Examining Committee of the Atmospheric Sciences' Bachelor of Science Programme of the Federal University of Itajubá (UNIFEI, MG, Brazil), as a partial requirement to obtain the title of
Bachelor of Science in Atmospheric Sciences

Tutor: **Vanessa Silveira Barreto Carvalho**
Co-tutor: **Arcilan Trevenzoli Assireu**

Itajubá, MG, Brazil
2015

Universidade Federal de Itajubá
Instituto de Recursos Naturais
Programa de Graduação em Ciências Atmosféricas

The Examining Committee, below signing, approves this
Monograph

**THE WIND ENERGY RESOURCE OF A LARGE TROPICAL
AQUATIC SYSTEM: HIGH RESOLUTION NUMERICAL
ASSESSMENT AND THE ATMOSPHERIC STABILITY EFFECTS TO
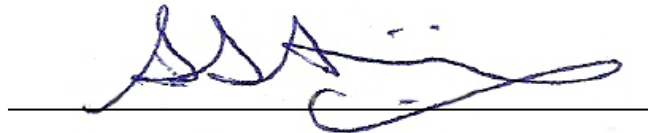POWER PRODUCTION**

by

Bruno de Campos

As a partial prerequisite to obtain the title of
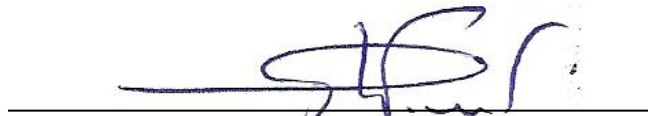
Bachelor of Science in Atmospheric Sciences

Examining Committee

Vanessa Silveira Barreto Carvalho, PhD (UNIFEI)
(Tutor)

Arcilan Trevenzoli Assireu, PhD (UNIFEI)
(Co-tutor)

Geraldo Lucio Tiago Filho, PhD (UNIFEI)

Michelle Simões Reboita, PhD (UNIFEI)

Itajubá, 19th of November 2015

ACKNOWLEDGMENTS

"Only two things are infinite, the universe and human stupidity, and I'm not sure about the former."

Albert Einstein

ABSTRACT

BSc Monograph
BSc Programme in Atmospheric Sciences
Universidade Federal de Itajubá, MG, Brazil

THE WIND ENERGY RESOURCE OF A LARGE TROPICAL AQUATIC SYSTEM: HIGH RESOLUTION NUMERICAL ASSESSMENT AND THE ATMOSPHERIC STABILITY EFFECTS TO POWER PRODUCTION

AUTHOR: BRUNO DE CAMPOS
TUTOR: VANESSA SILVEIRA BARRETO CARVALHO
Place and Presentation Date: Itajubá, 19th of November 2015.

This study aims to present the wind power resource assessment of the Furnas Reservoir, a comprehensive water body that can potentially lodge wind farms. It was performed a high resolution numerical experiment (3 km of horizontal resolution in the finer grid) using the Weather Research and Forecasting (WRF) model for a one-year run over 2014 in order to (a) validate the modelled data with observations from three anemometric towers installed in the area and (b) produce the wind power assessment based on the simulations output. Results show a good fit between modelled and observed data and good results when comparing the probability density function at the sites. Furthermore, the simulations also perform better under punctual synoptic events despite of the annual series. The assessment shows that the wind in the area tends to be stronger during spring and weaker during the winter, where the areas close to high elevations and under wind channelling conditions got the greatest values. Moreover, the wind speed variability is greater in the summer and spring. The average wind power density is also presented and can reach values up to 500 $W \cdot m^{-2}$ in certain areas. When evaluating the stability effects to power production – throughout the Richardson Number theory – results shows that power production can drop to almost 99% during stable atmospheric conditions and increase substantially during unstable conditions. Thus, it can be assumed that numerical weather prediction was an efficient tool in order to estimate the wind power resources in the study area and this study can conduct to further experiments related to power production, distribution and management in the study area.

Keywords: Furnas Hydroelectric Reservoir. Numerical weather prediction. WRF model. Wind power production. Weibull distribution.

FIGURES TABLE

TABLES LIST

LIST OF ABBREVIATIONS, ACRONYMS AND SYMBOLS

AFWA – Air Force Weather Agency

ANEEL – Agência Nacional de Energia Elétrica

AWPD – Average wind power density

BNDES – Banco Nacional do Desenvolvimento

CO_2 – Carbon Dioxide

DEM – Digital Elevation Model

DTE – Digital Terrain Elevation

FAA – Federal Aviation Administration

FSL – Forecast Systems Laboratory

GFS – Global Forecast System

GHG – Greenhouse Gases

IPCC – Intergovernmental Panel on Climate Change

kW – Kilowatts

MG – Minas Gerais

MM5 – Fifth-Generation Penn State/NCAR Mesoscale Model

MW – Megawatt

NASA – National Aeronautics and Space Administration

NCAR – National Centre for Atmospheric Research

NCEP – National Centres for Environmental Prediction

NEB – Northeast of Braszil

NWP – Numerical Weather Prediction

PBL – Planetary Boundary Layer

RAMS – Regional Atmospheric Modeling System

RH – Relative humidity

RMSE – Root-mean-square error

rpm – revolutions per minute

RRTM – Rapid radiative transfer model

SEB – Southeast of Brazil

SPD – Wind speed

SRTM – Shuttle Radar Topography Mission

TEMP – Air temperature

TKE – Turbulent Kinetic Energy

USA – United States of America

WDIR – Wind direction

WPA – Wind Power Assessment

WPR – Wind Power Resources

WRF – Weather Research and Forecasting

WMO – World Meteorological Organization

WWEA – World Wind Energy Association

d – Concordance coefficient

ρ – Correlation coefficient

g – Earth's gravity

Γ – Gamma function

Δz – Height increment

$\bar{\rho}$ – Mean air density

$\bar{\text{x}}$ – Mean value

o – Observation index

$\text{m} \cdot \text{s}^{-1}$ – Metres per second

P_A – Power availability

C_p – Power coefficient

A – Scale parameter, swept area

y – Simulation index

k – Shape parameter

σ – Standard deviation

$\Delta \bar{\bar{T}}_v$ – Virtual temperature increment

Δu – Horizontal wind speed increment

v – mean wind speed

SUMMARY

1. INTRODUCTION

Essentially, winds carry part of the energy received from the Sun through intermediate dynamical and physical processes occurring in the atmosphere. The uneven warming on surface and its pressure variations result in air displacement in the atmosphere. It can be assumed as an attempt to correct the natural gradients generated in the atmosphere (AHRENS, 2000).

During the past 50-60 years, the electric power generation has grown in most parts of the world (WWEA, 2014), driven by the steep uprising of the undeveloped countries. Thus, balance between access to energy, economic development and sustainability has shown up as the biggest challenge not exclusively to the observed countries but also to the global community. The necessity of natural resources and the impacts of power production do not have only local impacts but global consequences as well. The potential of producing energy using renewable resources, here on topic the wind power, can play the most important role against other sources, concerning the mitigation effects caused by climate change (WWEA, 2014). The Intergovernmental Panel on Climate Change (IPCC 2007) throughout its numerous scientific reports has found evidences that the climate in our planet is changing, potentially due to the human activities which trigger the accumulation of greenhouse gases (GHG) in the atmosphere. Between 1971 and 2010, the global emission of CO_2 nearly doubled and almost 44% of these emissions in 2000 came from the electrical sector. Still according to the IPCC, the wind power offers a significant potential on short-term (2020) and long-term (2050) in order to decrease the GHG emissions. The reduction of GHG is still one of the greatest motivations to the implementation of wind farms, due to the agreements signed by nations, aiming the collaborative reduction of GHG emission. The nations all around the world are facing energy security problems (*e.g.* risk of nuclear disposal leakage) and concomitantly looking for new solutions to environmental sustainability in order to plan a more diversified energy matrix, less dependent of exclusive sources (WISER et al., 2011).

According to ANEEL (2014), the term ''wind power'' can be obtained when considering the kinetic energy in the moving air masses (wind). Its role is on converting the translational kinetic energy to rotational kinetic energy via wind turbines (or also known as aero generators), to produce electric energy. Thereafter, the wind power assessment over one specific region requires a systematic methodology to

collect and analyse data, mostly wind speed and direction and their implication on the wind pattern. Usually, an assessment this size demands a specific data treatment, like airport datasets, seaports, weather stations and other similar sources of trusted data. These sources must be able to supply time series with enough quality in order to estimate the first attempts of raw energy potential or a theoretical overview in the study field (NREL, 2014; WINDUSTRY, 2015).

Any investor in wind power would admit to question how much energy a new project could produce in order to determine the economic viability of the new project on topic. Such information could interest several sources – investors, funders, project managers and public policies managers as well. In this process we should answer "what is the capacity and what is the energy produced" and such answering process is also known as "Wind Power Assessment" or more frequently "Wind Power (Potential) Assessment" (WPA). In this context, the set of techniques or methods used are similar, being different exclusively on the source of data and also concerning the applied methodology, mainly when dealing with local or global scales. The WPA takes in consideration not only the meteorological pattern of the variables but also some technical details concerning the equipment and machinery. Moreover, it is important to consider the final aim of the projects. The study can vary from micro scale to hundreds of thousands of kilometres.

In Brazil, the first electronic anemometers and special sensors to wind assessment were implemented at Ceará and Fernando de Noronha, in the early 90s. The products of such measurements were responsible to make the deterministic local wind power resource (WPR) possible and also the installation of the first turbines in Brazil. Moreover, these areas are the *avant garde* on WPR also due to the essential knowledge about the patterns of appropriate wind conditions all over.

In the country, the market has behaved in a promising and receptive way to new power matrixes. It can be estimated that in 2014 it had been invested R$ 15 bi in the wind power sector in Brazil. This baseline is expected to be kept to the next years (AGÊNCIA BRASIL, 2014). Still, in ten years the wind power will represent 11% of the Brazilian power matrix, aiming to keep the highest level of nationalization as possible, including the equipment manufacturing, a basic requirement to claim for funding from the Banco Nacional de Desenvolvimento Econômico e Social (BNDES).

The diversification of the energy matrix in a nation is vital to overcome economic and social crises as well as natural disasters which could affect the energy

production. In this context, Furnas has been playing an important role to solve the energy crises which had threatened Brazil in the 50s. Furnas Power Plant was the first big hydroelectric in Brazil, with capacity of 1216 MW, implemented in Rio Grande (MG) in 1958. In 1963, through the Federal Decree Number 41066, the company termed Central Elétrica de Furnas started its operations effectively, in Passos (MG) (PORTAL FURNAS, 2014). The reservoir has a surface of approximately 1440 km^2 and it is composed by two branches, east and southern from the dam. The lake's storage level is at 768 m with maximum quota of 769 m and operational level of 750 m above sea level. Due to its importance to the State and also to the whole Southeast of Brazil (SEB), the region is the focus of several renewable energy studies and other fields of science, aiming to make the most of their natural resources for production.

According to ANEEL (2014) and Grubb and Meyer (1993), in order to make the wind power serviceable, its density must be greater than 500 W/m^2 at a 50 m height, which requires minimum wind speeds around 7 to 8 m/s. To the World Meteorological Organization (WMO), such requirements can be found only at 13% of Earth's surface, reaching 32% in East Europe. Thus, one of the biggest challenges to elaborate a concise study about the wind power resources is the retrieving of trusted and systematic data at the study field. In Brazil, such patterns can be better observed in the Northeast, mostly alongside the coast (AMARANTE et al., 2001).

The study of renewable energy, more precisely wind power, are relatively new in Brazil and still need more attention, technologies and products in order to supply the high level of growth of the sector in the country. According to the Global Wind Energy Council, China, USA and Germany lead the global ranking of implemented capacity of wind power production (GEWC, 2015).

In this context, the atmospheric numerical modelling can be a more and more present tool for such studies, because it can offer a set of multi-dimensional data able to verify the wind behaviour – and other atmospheric variables as well – at several vertical levels and with horizontal resolution from hundreds of metres to hundreds of kilometres.

Nowadays, one of the most used numerical models, both for research purposes or operational runs, is the Weather Research and Forecasting (WRF) Model (SKAMAROCK et al., 2008). WRF is an atmospheric modelling system which covers numerous physical, dynamical and computational options. WRF can be applied to meteorological investigations, real time weather forecasts, idealized simulations and

studies in data assimilation and geophysical coupled models. The WRF model has a comprehensive community of users and developers, being present in more than 130 countries and counting with more than 25,000 users (WRF-MODEL.ORG, 2015). Nowadays, WRF is a system developed by the National Centre for Atmospheric Research (NCAR), National Oceanic and Atmospheric Administration (represented by the National Centres for Environmental Prediction (NCEP) and the Forecast Systems Laboratory (FSL), Air Force Weather Agency (AFWA), Naval Research Laboratory, University of Oklahoma, and Federal Aviation Administration (FAA).

The WRF ARW core has fully compressible, Euler non-hydrostatic equations, conservative for scalar variables. The vertical coordinate is a terrain-following, dry hydrostatic-pressure, with vertical grid stretching permitted, with the top of the model as a constant pressure surface and the horizontal grid as an Arakawa C-grid staggering. The time integration follows a time-split integration using a 2nd or 3rd order Runge-Kutta scheme with smaller time step for acoustic and gravity-wave modes. It includes full Coriolis terms and grid and observation nudging capabilities (SKAMAROCK et al., 2008).

In recent studies conducted abroad, Nawri et al. (2014), throughout a comprehensive report about the wind characteristics in Iceland, used WRF with 2 nested grids over the island with maximum resolution of 3 km. In order to verify the quality of the simulated data, they used datasets from several weather stations and reanalysis datasets from some European meteorological centres. The authors, when looking at regional comparisons and an identification of favourable areas to wind farms, they could define 14 test sites for a more detailed study, ranking the country as a high class of wind power production according to the European Atlas. Moreover, it can be observed that even small wind farms are able to produce as much power during the year as the hydraulic and thermal matrixes in operation.

Li et al. (2014) also adopted the WRF model in their studies for the coast of Liaoning (China) using observations from anemometric towers and a model setup of 1 km (horizontal resolution) over the region. The authors found relevant results between both methods on spring and summer, on all the wind parameters analysed. However, the model tends to overestimate such parameters in comparison to the anemometric towers. According to them this difference is associated to the bias in the initial and boundary condition in WRF, on autumn and summer: the global model overestimates

the winds on these seasons and the regional model follows this trend with badly-solved perturbations, transferring the errors from synoptic to mesoscale.

The wind power availability differs from other sources due to the stochastic nature of the wind (FOLEY et al., 2012). The authors revised several methods of investigation of wind power resources, with factors associated to global scale, local scale, possibilities of ensemble forecast and uncertainties in the prognostic techniques. Shimada e Ohsawa (2011) when using the WRF to study its accuracy and the behaviour of offshore winds, found a bias of 15.3% in the simulations in comparison with observed data, where the greatest errors were associated to the inefficiency of planetary boundary layer parameterizations.

Chin et al. (2010) tested WRF in several horizontal resolutions and with different physical configurations for five events of clear-sky condition, validating the results with observations. Greater resolutions are able to provide a better representation of mountain-and-valley breeze, with impacts on the final results. Furthermore, the physical parameterizations can show a significant difference in the final results, in question here the planetary boundary layer (PBL), surface and soil-layer schemes. Similarly, Draxl et al. (2010) selected seven physics schemes for the PBL using WRF and they evaluated its performance in order to study the wind patterns at 10, 40, 60, 80, 100, 116 and 160 metres above ground (turbine height), as well as the shape of the wind shear. Their results show that PBL schemes based on turbulence kinetic energy compare better with the observations and that the diurnal evolution and the expected transitions of wind speed, temperature and the α-parameter are well captured by all of the schemes, except for the YSU scheme.

De Foy et al. (2009) used the PSU/NCAR Mesoscale Model (MM5) and WRF model along with measured data, for an assessment of complex wind fluxes in the Metropolitan Region of Mexico City. Three methods were applied, the first one comparing the simulations with observations and the second and third ones using pollutant plumes to verify the model skill on the wind dispersion. The authors found better results with the WRF in relation to the MM5 and could conclude that numerical simulation have enough quality for this sort of work.

Deppe et al. (2013) implemented WRF with 10 km horizontal resolution in order to study its performance under a hypothetical turbine at 80 m height. The author used an ensemble forecast of several PBL parameterizations and verified a small bias in comparison to the single simulations. When inducing random disturbs in the initial

conditions it can be ascertained big differences in the isolated simulations, however with small bias in the ensemble.

In Brazil, some studies as cited below also used the numerical weather prediction (NPW) and also aimed to evaluate the available wind power resources of a certain area, as well as the wind patterns related to it. Other studies, presented next, have shown studies of wind profiles throughout other resources, such the ones with local anemometric stations only. There is still a lot to the investigated when dealing with the Brazilian wind power resources, because a lot of the job done is conducted in national scale by public agencies or big companies in the private sector, restricting the forecast to big areas.

Martins et al. (2007) show a revision of the physical concepts applied on the study of wind kinetic energy to produce electrical power. The author describes the dynamical characteristics of global circulation and discusses the main methodologies used in the NWP, including the numerical downscaling, statistical, physical downscaling, etc. The effects of wind intensification due to orographic forcing was studied by Assireu et al. (2013) with the WRF v3.2, where it can be presented the wind channelling in Furnas area due to the reservoir construction within the mountains. Recent studies propose that the Furnas Reservoir area is strongly affected by mesoscale and micro scale atmospheric disturbs, such as mountain waves (DE CAMPOS et al., 2015). Such phenomena may imply to an important impact to the power production as well. Valle et al. (2013) studied the PBL with a model applied to micro-regions in order to verify the best sites to implement a 10 kW generator in Sete Lagoas, MG.

Ramos et al. (2012) also use the WRF to the Alagoas State. The authors evidence a very satisfactory quality of the numerical simulations during the dry period in the State, with bias around 0.98 m/s and RMSE of 3.61 m/s. It's highlighted the necessity of more studies on cloud microphysics and cumulus parameterizations and it is concluded that WRF is a very useful tool to the WPA. Still in the NEB, Maria et al. (2008) utilized the Regional Atmospheric Modelling System (RAMS) model with three sets of horizontal resolutions and parameterizations in the finer grids (20, 5 and 1 km). The authors concluded that a finer resolution (1 km) agrees better with the observations in the Ceará coast, combined with the parameterized turbulence with an anisotropic version of the scheme proposed by Smagorinsky and Newtonian relaxation time of 12h.

Besides the study of the horizontal pattern of the wind, it is important to highlight the importance to investigate the mutable vertical wind profile to the wind assessment and a better understanding of the PBL. The PBL, or planetary boundary layer (ABL), is the lowest part of the atmosphere and it is directly influenced by its contact with the Earth's surface. The velocity decreasing near the surface is a function of surface roughness, so wind velocity profiles are fairly different for different terrain types.

As Navier–Stokes (motion) equations (shows, the planetary boundary layer turbulence is produced in the layer with the largest velocity gradients that is at the very surface proximity. This layer – also known as surface layer – constitutes about 10% of the total PBL depth. Above the surface layer the PBL turbulence gradually dissipates, losing its kinetic energy to friction as well as converting the kinetic to potential energy in a density stratified flow. The balance between the rate of the turbulent kinetic energy production and its dissipation determines the planetary boundary layer depth (HOLTON, 2004). In general, the PBL depth varies usually around 1 km, but in mid-latitudes it can vary from 100 m to 3 km and the temperatures vary diurnally, unlike in the free atmosphere above. The surface influences the PBL by friction and by heat fluxes at the ground and it is characterized by turbulence, which is generated by wind shear. Temperature gradients can either generate or suppress turbulence. We can also define the Boundary layer clouds as a region with predominantly fair-weather cumulus, stratocumulus and fog (HOLTON, 2004).

The characterization of the PBL also depends on its stability, instability and neutral conditions, in association with temperature and wind profiles over a specific region. One of these indicators in the PBL is R_i, or the bulk Richardson number (LACKMANN, 2012). It is a dimensionless number that expresses the ratio of the buoyancy term to the flow gradient term.

The R_i has been extensively used as a parameter to measure the stability of PBL (STULL, 1988). In unstable conditions, the wind shear parameter overlaps the thermally produced turbulence and R_i becomes negative. In stable condition, the thermally produced turbulence is dominant over wind shear and R_i becomes positive. Under conditions close to neutrality R_i assumes values between zero and one.

Some authors studied the vertical fluxes in the atmosphere as well as the conditions leading to instability. They also applied the Richardson concepts about the Monin-Obukhov theory (MONIN and OBUKHOV, 1954; FOKEN, 2006). The aim is

to establish a relation between the vertical wind profiles in any atmospheric condition and everywhere as a function of the surface fluxes. As example, Khanna & Brasseur (1997) studied the previsibility of the Monin-Obukhov similarity theory in regions close to surface. The authors analysed moderate and neutral instability conditions with large-eddy simulations. Pahlow et al. (2001) collected combined data from several campaigns of a field experiment in order to get a better understanding of turbulent structure from a stable PBL. It was observed a mismatch between the production and dissipation of turbulent kinetic energy (TKE) close to the limit of quasi-neutrality.

In this context, this work aims to determine the wind power resources of the Furnas reservoir throughout a study of the wind patterns in a high resolution simulation scheme where WRF model will be used for a one-year run. Moreover, this work aims to define the impact of the PBL instability conditions on the wind power production as well as the wind circulation patterns over the area. The importance of this study is to get a better understanding of the off-shore characteristics applied to power production, as well as the behaviour of the PBL in several atmospheric conditions.

2. MATHERIALS AND METHODS

2.1. Study area

The numeric experiment and observations were conducted over the Furnas reservoir area, located in the Minas Gerais State, southeast of Brazil. The reservoir covers an area of about 1440 km^2 with a maximum quota of 762 m (from sea level) and comprehends 34 counties in the State. The lake is formed by two branches, east and southern. It is considered one of the biggest reservoirs in Brazil. The reservoir location is shown in Figure 1 and the Digital Terrain Elevation (DTE) from Global Mapper® for the area is presented in Figure 2. The terrain data is derived from the NASA Shuttle Radar Topography Mission (SRTM; JARVIS et al., 2008) with 1 arcsec of horizontal resolution.
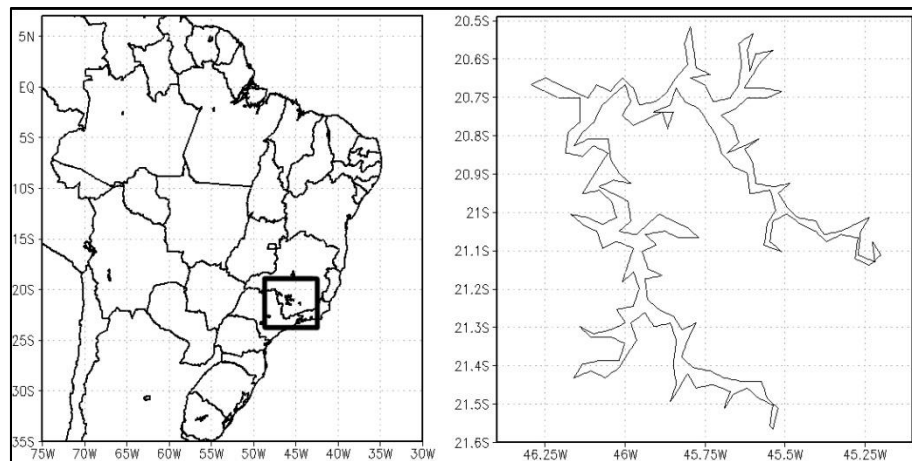

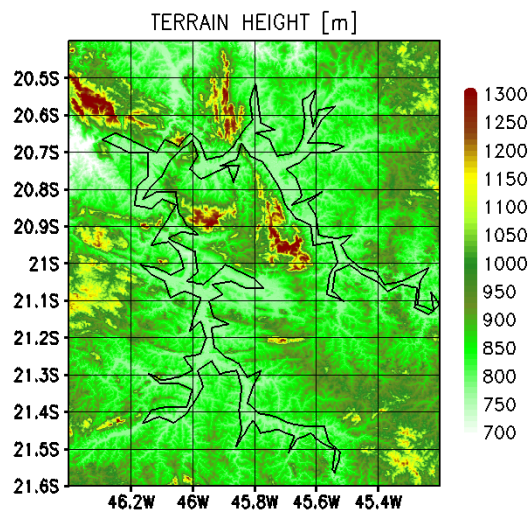**Figure 1**: Location of the Furnas reservoir zoomed over the Brazilian southeast region.

Figure 2: Digital Terrain Elevation at the Furnas Reservoir.

2.2. Model description and simulations

The WRF model was chosen for the simulations, with three nested grids with 27, 9 and 3km (finer domain) of horizontal resolution, centred over the Furnas reservoir according to Figure 3. The physical setup is described in Table 1. The model was initiated with the Global Forecast System (GFS; NCEP, 2015) analysis with 0.5° of horizontal resolution and 6h of temporal resolution, for the boundary and initial conditions.

The model was integrated monthly, from December 2013 to November 2014, totalizing one year of simulation. In every run (monthly) the model is initiated 24 hours prior the month of analysis and the first 24 hours are discarded in order to avoid the model numeric spin-up errors (SKAMAROCK, 2004). The simulated wind fields were extracted at 3, 10, 20, 40 and 120 m height on the model vertical coordinate. The air temperature and relative humidity timeseries were extracted at 3, 10, 20 and 40 metres.
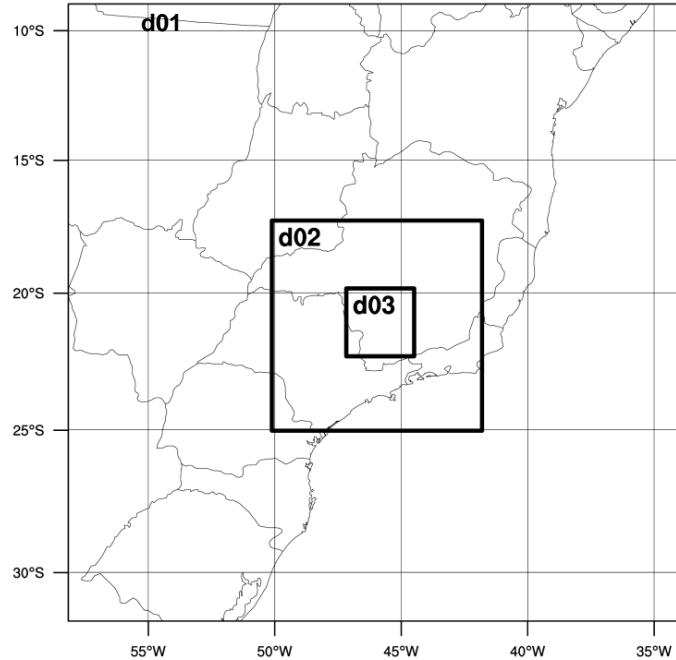

Figure 3: WRF domains setup.

Table 1: Model setup and physical parameterizations.

parameter	grid 1	grid 2	grid 3
points in x direction	95	97	94
points in y direction	95	97	94
total ETA levels	40	40	40
horizontal resolution	27 km	9 km	3 km
time step	75s	25s	8,3s
central latitude		-20.73	
central longitude		-45.96	
microphysics		Lin	
cumulus		Kain-Fritsch (d01, d02)	
planetary boundary layer		YSU	
surface		Monin-Obukhov	
short wave radiation		Dudhia	
long wave radiation		RRTM	

2.3. Observed dataset and data validation

In order to validate the simulations it were used three anemometric towers with minutely data where the timeseries were averaged into hourly series aiming to compare them with the model outputs.

The first weather station (alias "T42M") is a 42 metres height tower with sensors at 3 m, 10 m, 20 m, and 40 m, providing air temperature (TEMP), relative humidity (RH), wind speed (SPD) and wind direction (WDIR) datasets. The second and third ones ("TILHA" and "TTMR", respectively) provide the same parameters at 10 m height only. Their location is presented in Table 2. Their locations and surroundings are presented in Figure 4 as well, with the Digital Elevation Model (DEM). T42M and TILHA have data available from May/2014 to Aug/2014 and TTMR data on Jan/2014 and from Apr/2014 to Jun/2014. It is important to highlight that we filtered the data prior due to some unrealistic values in the observations related to bad recordings and other issues in the instruments. Thus, the simulated results were paired to match the dates in the observed datasets.
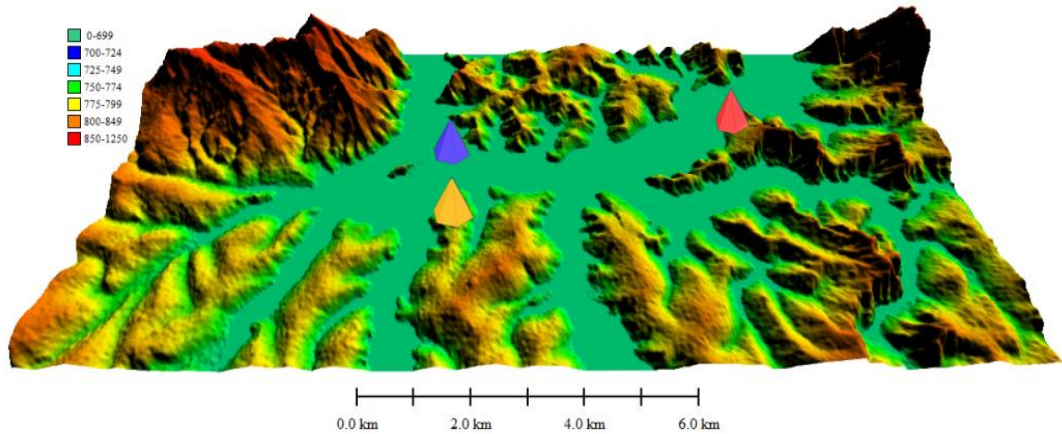
Figure 4: Location of the anemometric towers, trimmed from the reservoir domain area, where the yellow pyramid represents T42M, the blue one represents the TILHA station and the red one, TTMR.

Table 2: Anemometric tower coordinates.

NAME	LATITUDE	LONGITUDE
T42M	20.740440 °S	45.957700 °W
TILHA	20.730415 °S	45.963173 °W
TTMR	20.719491 °S	45.881849 °W

For the statistical and comparative analysis between simulation and observation we calculated: (a) mean ($\bar{x}$), (b) standard deviation (σ), (c) root of mean squared error (RMSE), (d) correlation coefficient (ρ), and (e) concordance correlation coefficient (d; WILLMOT, 1981) following the equations in Table 3, where (y) is assigned to the simulation parameters and (o) to the observed ones. To evaluate the model skill, the criteria established by PIELKE (2002) were analysed and a good skill can be said as a good match between observed and simulated standard deviations (I), RMSE less than the observed standard deviation (II) and $RMSE_{UB}$ less than the observed standard deviation (III), following:

$$\sigma_{sim} \cong \sigma_{obs} \qquad\qquad\qquad (I)$$

$$RMSE < \sigma_{obs} \qquad\qquad\qquad (II)$$

$$RMSE_{UB} < \sigma_{obs} \qquad\qquad\qquad (III)$$

Moreover comparative wind-rose between observation and simulation was generated for all the stations at their specified vertical level as well as the Weibull

distribution (Equation 1) of wind at the sites, seasonally and annually. The Weibull distribution (WEIBULL, 1951; Equation 1) is most commonly employed for wind energy studies (MORGAN et al., 2011), mostly for off-shore wind assessments and constitutes the most widely accepted distribution for wind speed. In this study we derived the Weibull estimators from the numerical methods of MATLAB® (MATHWORKS, 2012). Hereafter, *A* is the scale parameter (greater than zero, in units of wind speed) and the non-dimensional shape parameter *k* > 1.

Table 3: Statistical equations.

$\sigma = \sqrt{\dfrac{1}{n}\sum(x_i - \bar{x})^2}$	$RMSE = \sqrt{\dfrac{1}{n}\sum(y_i - o_i)^2}$
$\rho = \dfrac{\sum[(y_i - \bar{y})(o_i - \bar{o})]}{\sqrt{\sum(y_i - \bar{y})^2}\sqrt{\sum(o_i - \bar{o})^2}}$	$d = 1 - \dfrac{\sum(y_i - o_i)^2}{\sum(\,|y_i - \bar{o}| - |o_i - \bar{o}|\,)^2}$
$RMSE_{UB} = \sqrt{\dfrac{1}{N}\sum[(y_i - \bar{y}) - (o_i - \bar{o})]^2}$	

$$f(s; A, K) = \frac{k}{A}\left(\frac{s}{A}\right)^{k-1} e^{\left[-\left(\frac{s}{A}\right)^k\right]} \tag{1}$$

In order to test the model skills on simulating the atmosphere under two distinct synoptic events, we chose (a) a period with a cold front passing and (b) a period with the area under the effects of a high pressure system. For both, we computed – at TILHA location – the wind speed distribution and the wind-roses, using the simulated and observed datasets. According to the Centre for Weather Forecasting and Climate Research (CPTEFC-INPE), the high pressure system occurred between 11 and 14/05/2014. The cold front took place between 24 and 27/07/2014.

2.4. Wind power assessment

Once done the results validation at the sites, we begin the wind power assessment with the simulations output only. Furthermore, in order to evaluate the power generation on a more realistic scenario, it was selected the technical specificiations of ENERCON® E-82 turbine, whose description is presented in Table 4.

Table 4: Technical data of ENERCON® E-82.

PARAMETER	FEAUTURES
rated power	2,000 kW
rotor diameter	82 m
hub height	~120 m
turbine concept	Gearless, variable speed, single blade adjustment
number of blades	three
swept area	5,281 m²
rotational speed	variable, 6 - 17.5 rpm
cut-out wind speed	28 - 34 ms^{-1} (with ENERCON® storm control)

Thus, the following analyses were performed:

a) Annual and seasonal wind speed profile plots with the Weibull distribution at turbine height, mean wind speed (Equation 2), variance, shape and scale parameters at TILHA site. The mean wind speed (Equation 2), as a function of the gamma function (Γ; Equation 3), is presented below. The gamma function can be defined to be an extension of the factorial to complex and real number arguments.

$$\mu = A\,\Gamma\left(1 + \frac{1}{K}\right) \tag{2}$$

$$\Gamma(t) = \int_{-\infty}^{\infty} x^{t-1} e^{-x}\ dx \tag{3}$$

b) Mean wind speed maps at turbine level over the entire Reservoir, based on the Weibull mean function (Equation 4).

$$\bar{\mu} = A \int_{-\infty}^{\infty} \left(1 + \frac{1}{K}\right)^{t-1} e^{-\left(1 + \frac{1}{K}\right)}\ dx \tag{4}$$

c) Annual and seasonal wind-rose plots at 120 m (E-82 turbine level) with 30º sectors at TILHA location. We selected the TILHA coordinate to evaluate the

time series due to its location related to the wind intensification caused by orographic forcing (ASSIREU et al., 2013).

d) Scale parameters maps (k) at turbine level over the entire Reservoir, based on the Weibull, derived from the MATLAB® numerical approximations and estimators.

e) Annual and seasonal average wind power density (AWPD; Equation 5) plots at turbine level, where $\bar{\rho}$ is the average air density, in this work set as 1.225 kg·m^{-3}, v the mean wind speed and Γ is the gamma function, defined above in Equation 3. This method is based on the assumption that the density is not correlated with the wind speed (HANNESSEY, 1977; CARILLO et al., 2014).

$$AWPD = \frac{1}{2}\bar{\rho}v^3\Gamma\left(1 + \frac{3}{K}\right) \tag{5}$$

f) Annual and seasonal wind power availability (P$_A$; Equation 6) plots at turbine level, where v is the mean wind speed [m/s], A is the swept area and C_p represents the E-82 power coefficient for each wind speed range, as described in Figure 5.
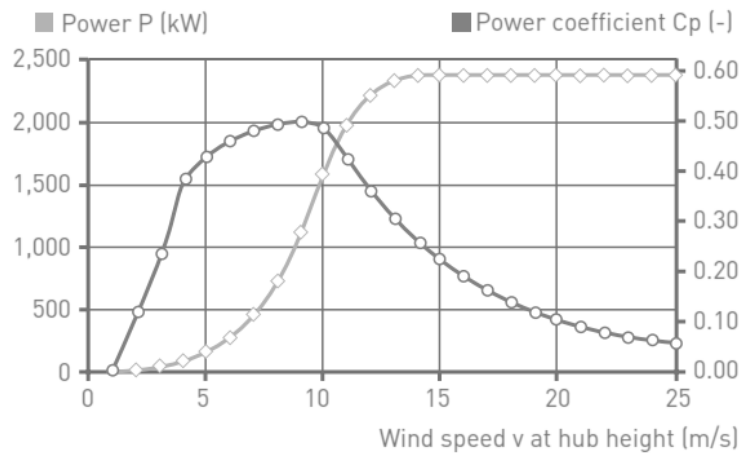
$$P_A = \frac{1}{2}\rho A v^3 C_p \tag{6}$$

Figure 5: Power Coefficient (C_p) evolution according to the wind speed at E-82 turbine level.

g) Annual and seasonal impact of power availability at turbine height subjected to stability conditions at TILHA. The instability/stability method follows the Richardson's theory (Equation 7) previously described. Below, θ_v, g, z, $\bar{u}$ and $\bar{v}$ represent the virtual temperature, gravity parameter, height, mean zonal wind and mean meridional wind, respectively. It was computed the percentage of the anomalies of P_A for the atmosphere under stable, unstable and neutral conditions, considering the annual mean as well as the summer, autumn, winter and spring means. In unstable conditions, the wind shear parameter overlaps the thermally produced turbulence and R_i becomes negative. In stable condition, the thermally produced turbulence is dominant over wind shear and R_i becomes positive. Under conditions close to neutrality R_i assumes values between zero and one.

$$R_i = \frac{\frac{g}{\theta_v}\left(\overline{\frac{\partial \theta_v}{\partial z}}\right)}{\left(\frac{\partial \bar{u}}{\partial z}\right)^2 + \left(\frac{\partial \bar{v}}{\partial z}\right)^2} \tag{7}$$

3. RESULTS AND DISCUSSION

3.1 Data Validation

Table 5 presents statistical results for TTMR when comparing the simulation with observations. It can be noticed very close values when analysing the means of all variables. However the values of correlation and concordance are not satisfactory. According to the skill test presented in Table 3, the three variables partially passed, mostly due to the discordances in the standard deviations and the RMSE. Similarly, for TILHA (Table 6) better results were founded for all the three variables. The TEMP and RH passed on all skill conditions and SPD was partially approved, due to the $RMSE$ and $RMSE_{UB}$.

Table 5: Statistics for data comparison at TTMR.

	variable	$\overline{x}_y$	$\overline{x}_o$	σ_y	σ_o	$RMSE$	ρ	d	$RMSE_{UB}$
10 m	**TEMP**	22.42	24.47	5.03	3.52	5.30	0.39	0.46	4.88
	RH	71.11	65.97	15.46	15.02	15.40	0.55	0.67	14.52
	SPD	3.61	3.52	2.01	2.13	2.52	0.26	0.41	2.52

Table 6: Statistics for data comparison at TILHA.

	variable	$\overline{y}$	$\overline{x}$	σ_y	σ_x	$RMSE$	ρ	d	$RMSE_{UB}$
10 m	**TEMP**	18.94	19.66	2.63	3.17	2.01	0.81	0.87	1.88
	RH	78.07	73.28	15.29	14.79	12.30	0.72	0.81	11.32
	SPD	3.01	2.71	1.81	1.89	1.96	0.45	0.61	1.94

The Table 7 shows the data validation at T42M for its four vertical levels. The results at 3 m are satisfactory and the skill test is partially filled for all the variables. The data show a good fit when analysing the correlation coefficient and the concordance parameter. At 10 m, TEMP and RH totally pass the skill test and SPD partially passes it. Once again the results are satisfactory however ρ and d are less precise than at 3 m height. At 20 m the skill test is partially fulfilled for all variables and it can be noticed a very unsatisfactory result from the wind speed analysis. At 40 m, TEMP and RH pass in all skill tests and SPD partially passes. The means and standard deviations at 20 and 40 m are less fit than at 3 and 10 m.

Table 7: Statistics for data comparison at T42M.

	variable	$\overline{y}$	$\overline{x}$	σ_y	σ_x	$RMSE$	ρ	d	$RMSE_{UB}$
3 m	**TEMP**	19.85	21.39	3.00	3.25	2.31	0.85	0.85	1.72
	RH	73.08	62.31	16.55	14.83	15.78	0.73	0.71	11.53
	SPD	2.71	2.67	1.58	1.59	1.79	0.36	0.53	1.79
10 m	**TEMP**	19.78	21.62	3.00	3.23	2.52	0.85	0.82	1.72
	RH	71.75	66.04	16.88	18.21	15.36	0.67	0.77	14.26
	SPD	3.12	2.02	1.80	1.13	2.11	0.31	0.23	1.80
20 m	**TEMP**	19.73	21.66	3.03	3.25	2.63	0.84	0.81	1.80
	RH	70.91	61.73	17.34	14.59	15.00	0.74	0.75	11.87
	SPD	3.36	4.67	1.94	2.47	3.19	0.15	0.10	2.91
40 m	**TEMP**	19.54	21.57	3.11	3.19	2.67	0.85	0.80	1.74
	RH	70.04	62.37	18.10	15.02	14.36	0.75	0.78	12.14
	SPD	3.70	2.49	2.17	1.46	2.50	0.32	0.29	2.19

The comparison of simulated and observed probability distributions of wind speed is presented in Figure 6. We can notice a very good fit for TTMR (a), TILHA (b) and T42M at 3 m (c). Despite their correlation coefficient have not shown such good results in the previous analysis we can observe a good fit for the distribution, more relevant for the WPA. For T42M at 10m (d) and 40m (f) the simulations tend to overestimate the wind speed and its distribution to higher speeds. At 20 m (e), the model tends to underestimate them.

Such results agree with other studies. The South Baltic Wind Atlas (RISØ-R-REPORT, 2011) found a better fitting between WRF and observations when analyzing the lower-levels timeseries in the validations. However, their results show a good fitting and better correlations, since the numerical experiment was conducted at the Denmark surroundings, a flatter area, less affected by steep terrains and abrupt changes in roughness and energy balance.

The wind direction pattern at TTMR location (Fig. 7) shows a more predominant flow from NNE in the simulations and from NE. The wind speeds are also higher in the TTMR dataset. For TILHA (Fig. 7) both simulation and observation present a very similar pattern, however the observations (Fig. 8a) has a substantial frequency of winds from SSW which was not captured in WRF (Fig. 8b).
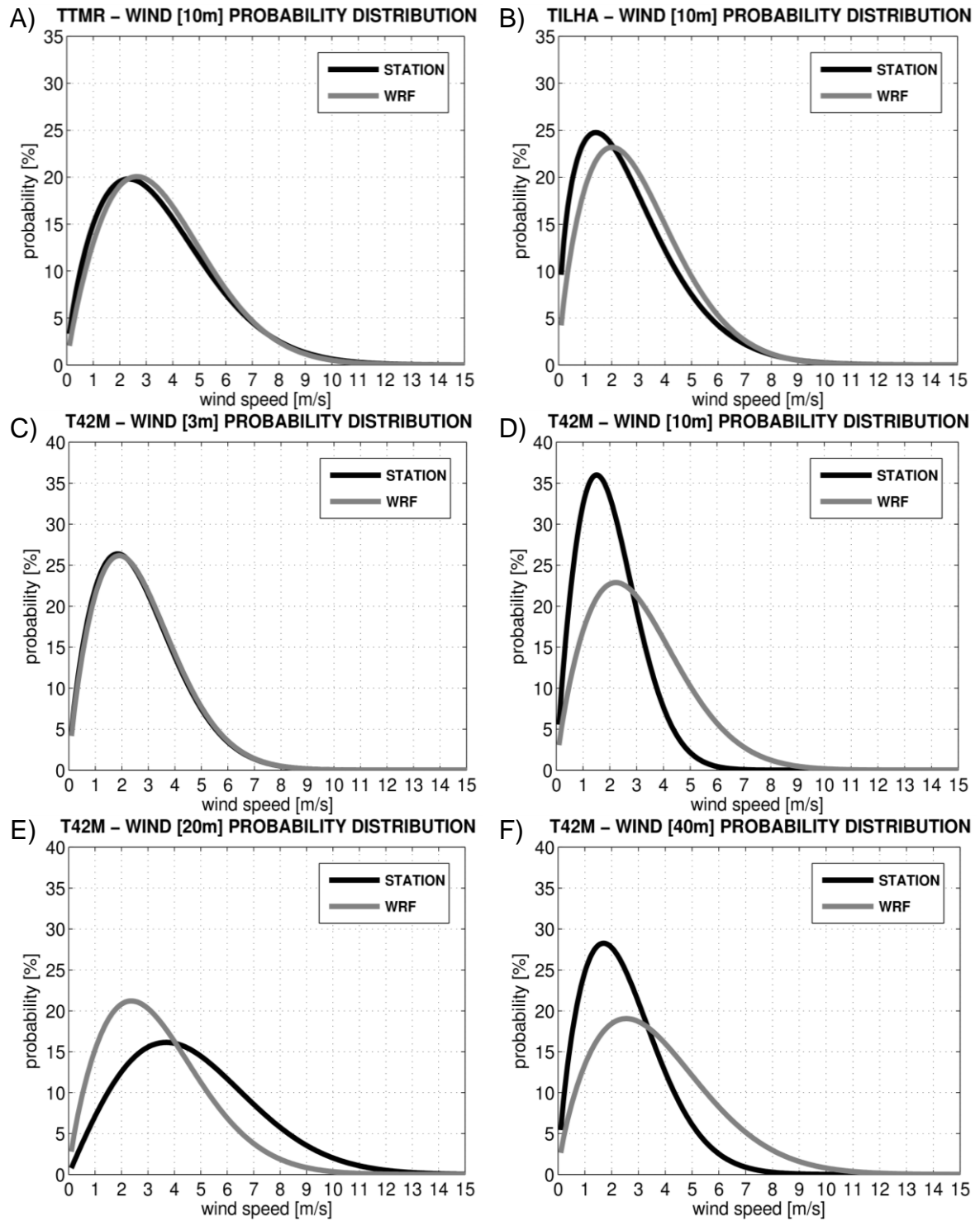
Figure 6: Data comparison of wind speed distributions for TTMR (a), TILHA (b) and T42M (c, d, e, f) from modelled and observed datasets.
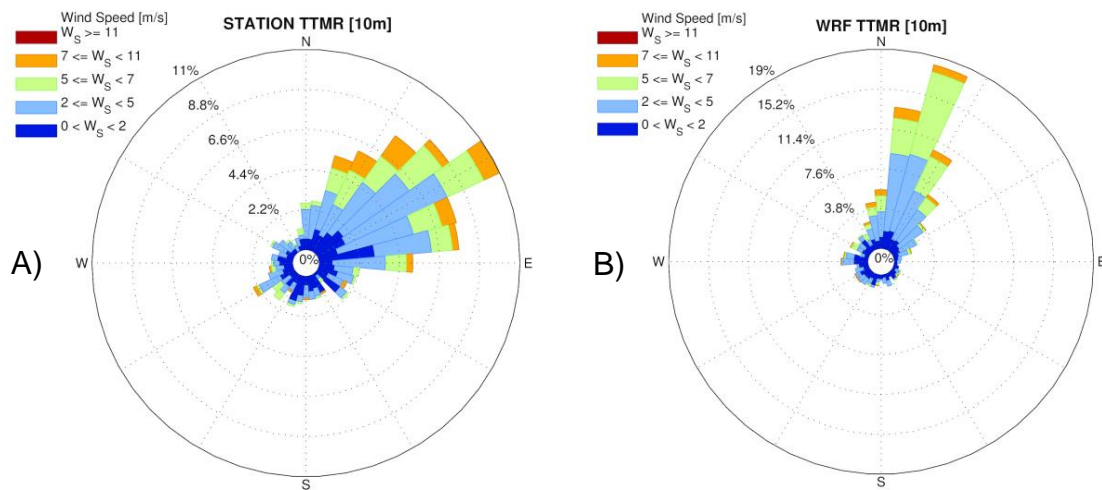
Figure 7: Wind roses comparison from TTMR (a) and WRF (b) at TTMR location.
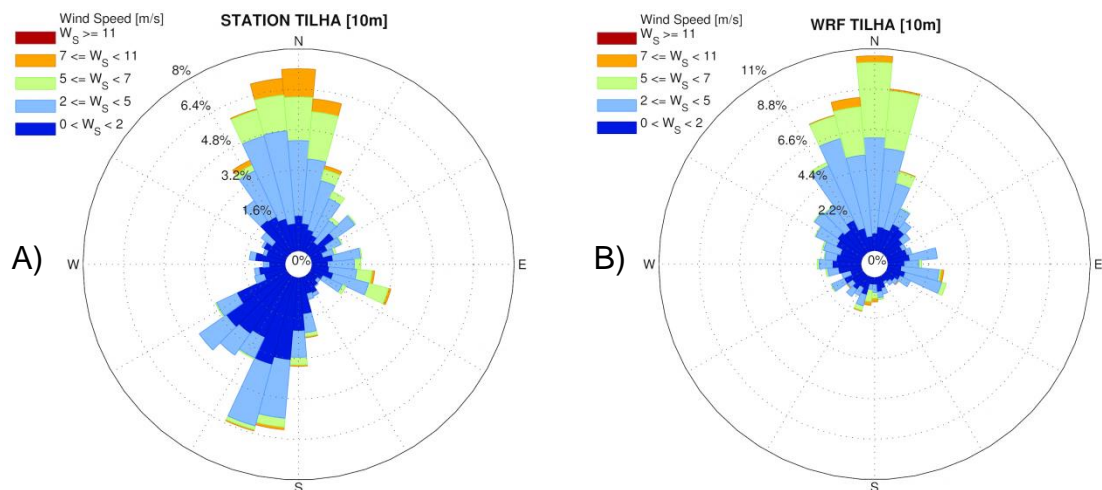

Figure 8: Wind roses comparison from TILHA (a) and WRF (b) at TILHA location.

The T42M site results for all the period of available observed data (Fig. 9) shows a predominant northerly pattern from WRF for all vertical levels, as well as the expected increase of frequency of higher speeds with height. For the observations, we can see a predominant pattern of north-easterly winds. Moreover, WRF shows more intense winds in the distributions, more evident at 40m.
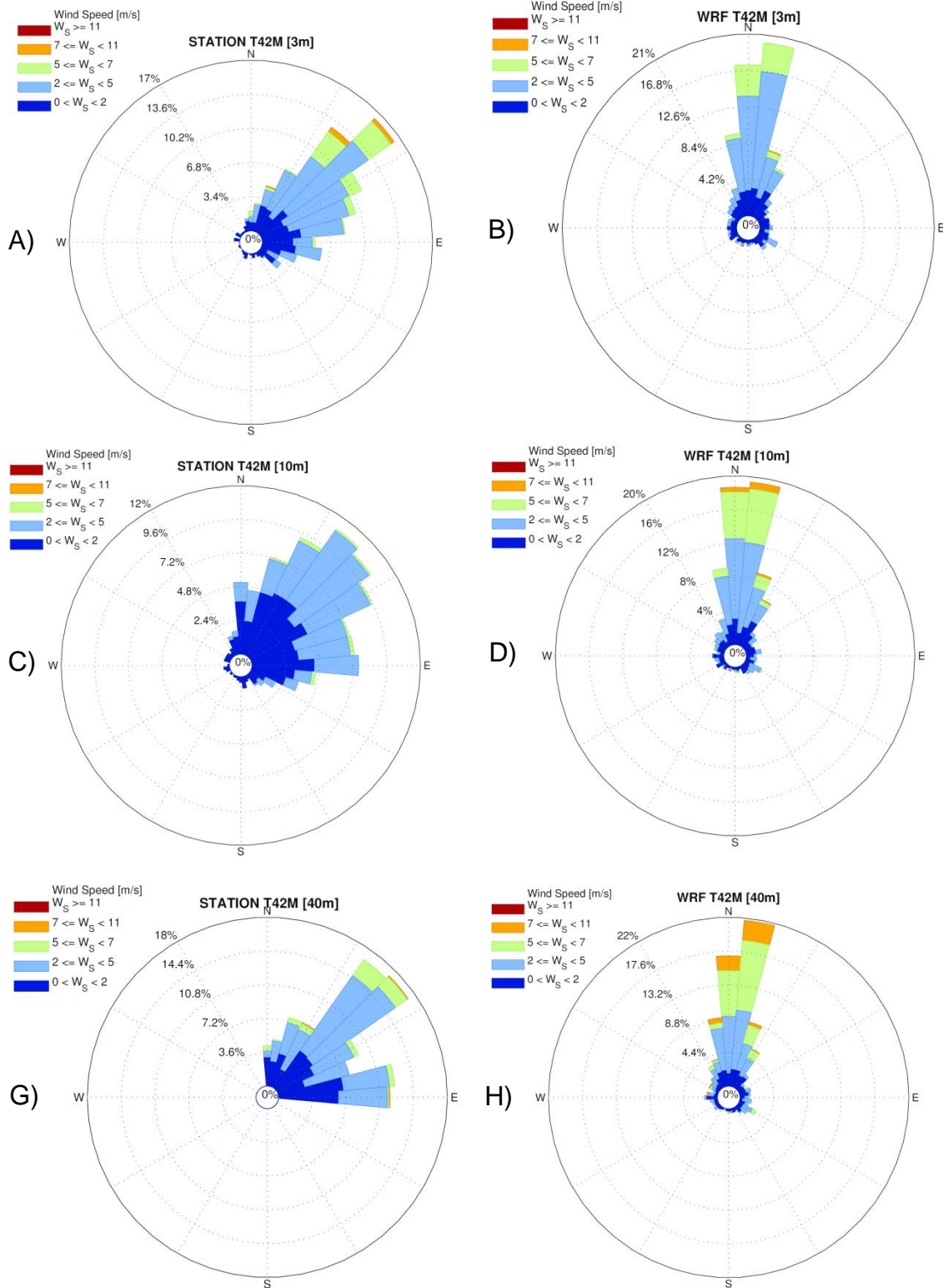
Figure 9: Wind roses comparison from T42M (a, c, e, g) and WRF (b, d, f, h) at T42M location.

3.2 Data validation under distinct synoptic conditions

In Figure 10 we can see the data fitting at TILHA for the (a) high pressure system episode and the (b) cold front passing. It is clear that the results for the high pressure system episode show better results than the ones for the cold front passing. The wind variability during a cold front may imply on the quality of simulations due to the wind gusts, difficult to predict and a great contributor to the expected errors. Contrariwise, an atmosphere under high pressure systems are designed to have more well-behaved wind patterns and the local circulation take place.
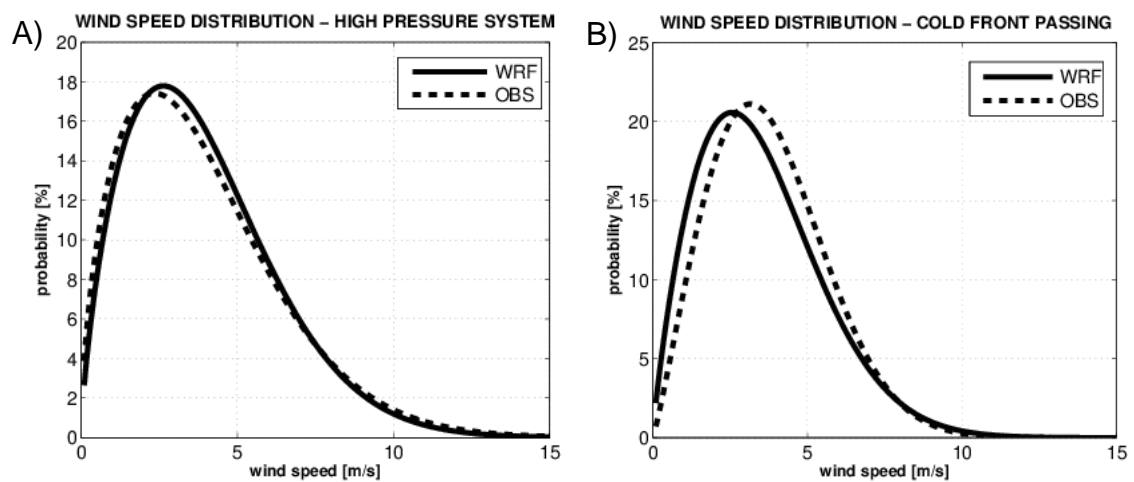

Figure 10: Data comparison of wind speed distributions for TILHA for the (a) high pressure system episode and the (b) cold front passing.

In Figure 11 and 12, we have the wind-roses for both periods presented above. WRF is able to find the most representative wind directions and speeds. However, the model tends to avoid the southerly winds from the high pressure event and it greats other minor directions during the cold front passing. The results and satisfactory and that may be an evidence that WRF can be more skilled during punctual events – such as cold fronts and high pressures – and less skilled on an annual analysis due to the amount of information contained and its implications to the statistics.
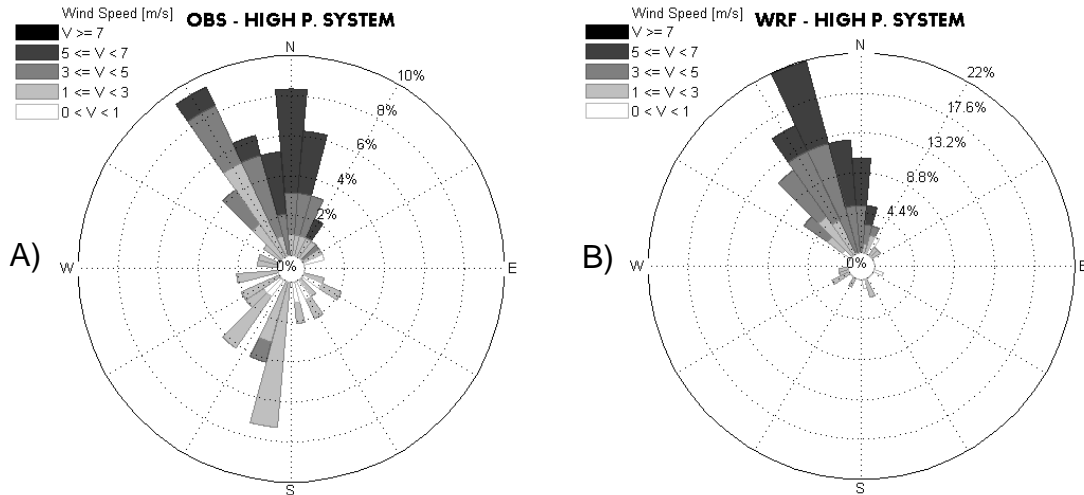
Figure 11: Wind-roses for the high pressure system episode at TILHA. Comparison between (a) observations and (b) simulation.
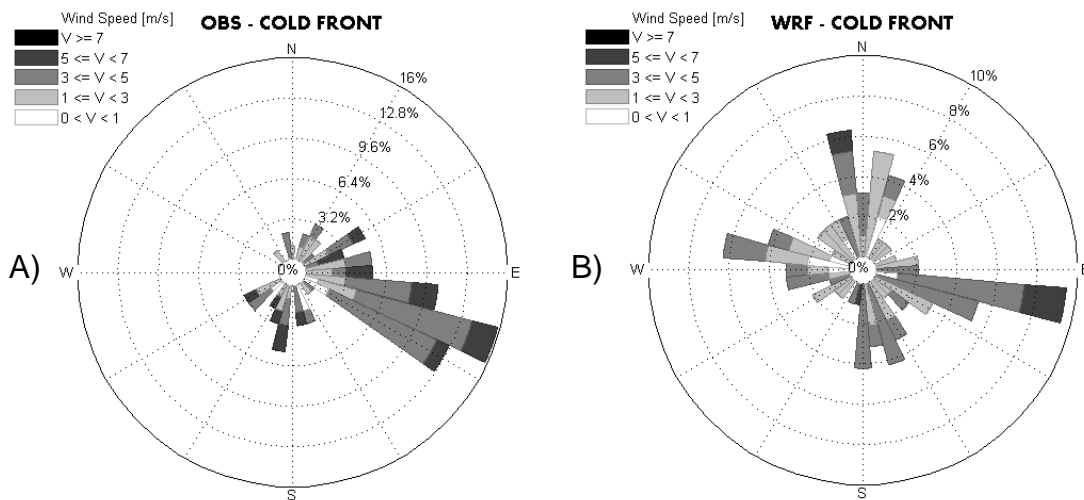

Figure 12: Wind-roses for the cold front passing at TILHA. Comparison between (a) observations and (b) simulation.

3.3 Wind Power Resources

This next section will investigate the wind power resources in the study field according to the WRF outputs. Figure 13 shows the wind speed distribution (following the Weibull distribution) at 120 m for the annual and seasonal timeseries at the TILHA coordinate. During spring we have the highest wind speed mean as well as the highest distribution of stronger winds. During the winter we have the weakest winds as well as a higher frequency of less strong winds. The annual and autumn profiles showed a similar patter, set in an average position between spring and summer.
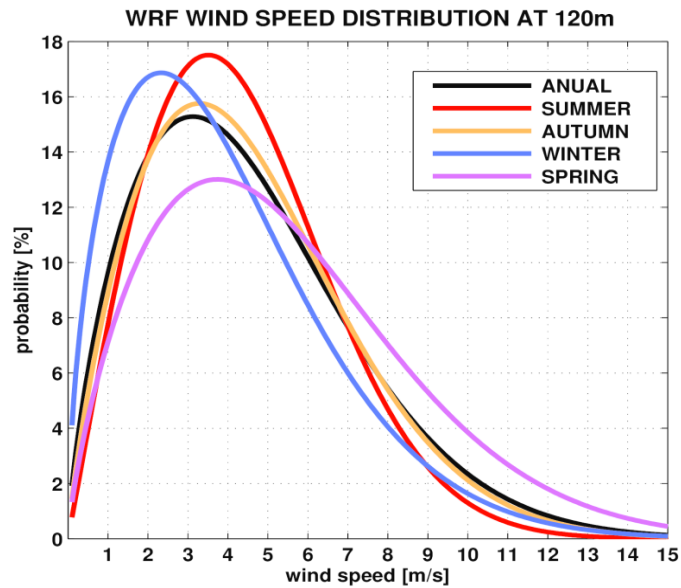
Figure 13: Probability distribution of wind speeds at TILHA site.

In Table 8 Weibull parameters are presented and results calculated for Figure 13. As the shape parameter (*k*) is considerably close in all the time periods presented, the scale parameter (*A*) becomes dominant. The highest value during spring proofs the distribution to higher wind speeds. The spring also has the greatest mean value of wind speed as well as the greatest variance. The annual timeseries has a satisfactory wind speed value for power producing.

In Figure 14 we can see the mean wind speed maps. The areas surrounded and the highest terrain elevations result in higher wind speeds. In addition, it is clear the greatest mean wind speed during the spring (Fig. 14e), with values up to 9 m.s^{-1}. The annual values are averaged with the other season's results and the intense values during spring become less dominant in the annual average. Furthermore, the minimum wind speed required in order to make the wind generation feasible is around 7 m/s (GRUBB and MEYER, 1993), which can be an evidence of the study area capabilities to wind power production.

Moreover, the wind roses at TILHA from the WRF dataset are presented in Figure 15. We can see a predominance of northerly winds in the annual and seasonal datasets.

Table 8: Weibull parameters at TILHA location from WRF simulations.

	A	k	$\bar{\bar{x}}$	σ^2
ANUAL	5.153	1.726	4.59	7.52
SUMMER	4.928	2.018	4.37	5.13
AUTUMN	5.127	1.812	4.56	6.78
WINTER	4.474	1.562	4.02	6.91
SPRING	6.090	1.747	5.42	10.26

Annual and seasonal shape parameters (k) are presented in Figure 16. The shape parameter defines how your data are distributed, but does not affect the location (on the x-axis) or scale of our distribution. A larger shape value gives a left-skewed curve, whereas a smaller shape values gives a right-skewed curve. Summer (16b) and winter (16d) hold the extremes, with maximum during summer, which means that the season has the greatest variability in the wind speed. The areas with maximum values of k also match the areas with the strongest wind speeds as presented in Figure 14. The annual mean (16a) is a balance between summer and winter. The transition seasons (autumn and spring) show very similar patterns between each other.

In Figure 17 annual and seasonal plots of average wind power density at 120 m over the Furnas reservoir are shown. The power density has its lowest values during autumn and summer and it is the greatest during spring, closely related to the stronger winds in that season. The values can reach up to 500 W/m^2 in certain areas. The greatest productivity lies in areas matching the mountains and their valleys. In general, it can be observed a low production over the lake, except for the area surrounded by the division between the two branches where the power density can reach up to 300 W/m^2 in the annual mean, following the mountains beside.

The similar analysis can be done for the wind power availability (Fig. 18). We have a maximum during spring with values up to 1.5 MW close to the mountains and the valleys over the reservoir area and surroundings. The poorest values are found during autumn and the annual mean shows a low production over the lake, except for the division between the two branches, with values up to 0.7 MW.
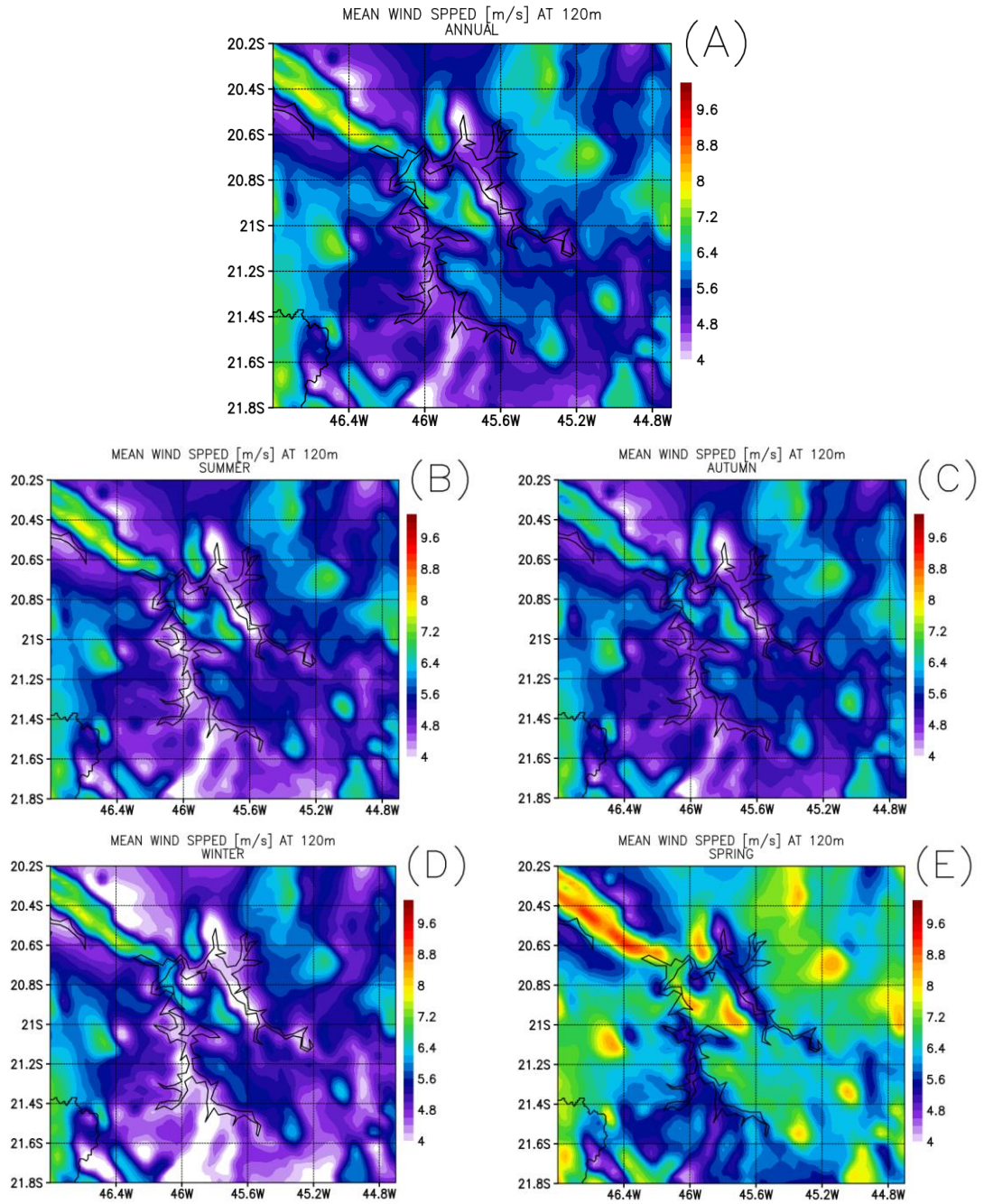
Figure 14: Average wind speed at 120 m based on the Weibull distribution. Seasonal and annual.
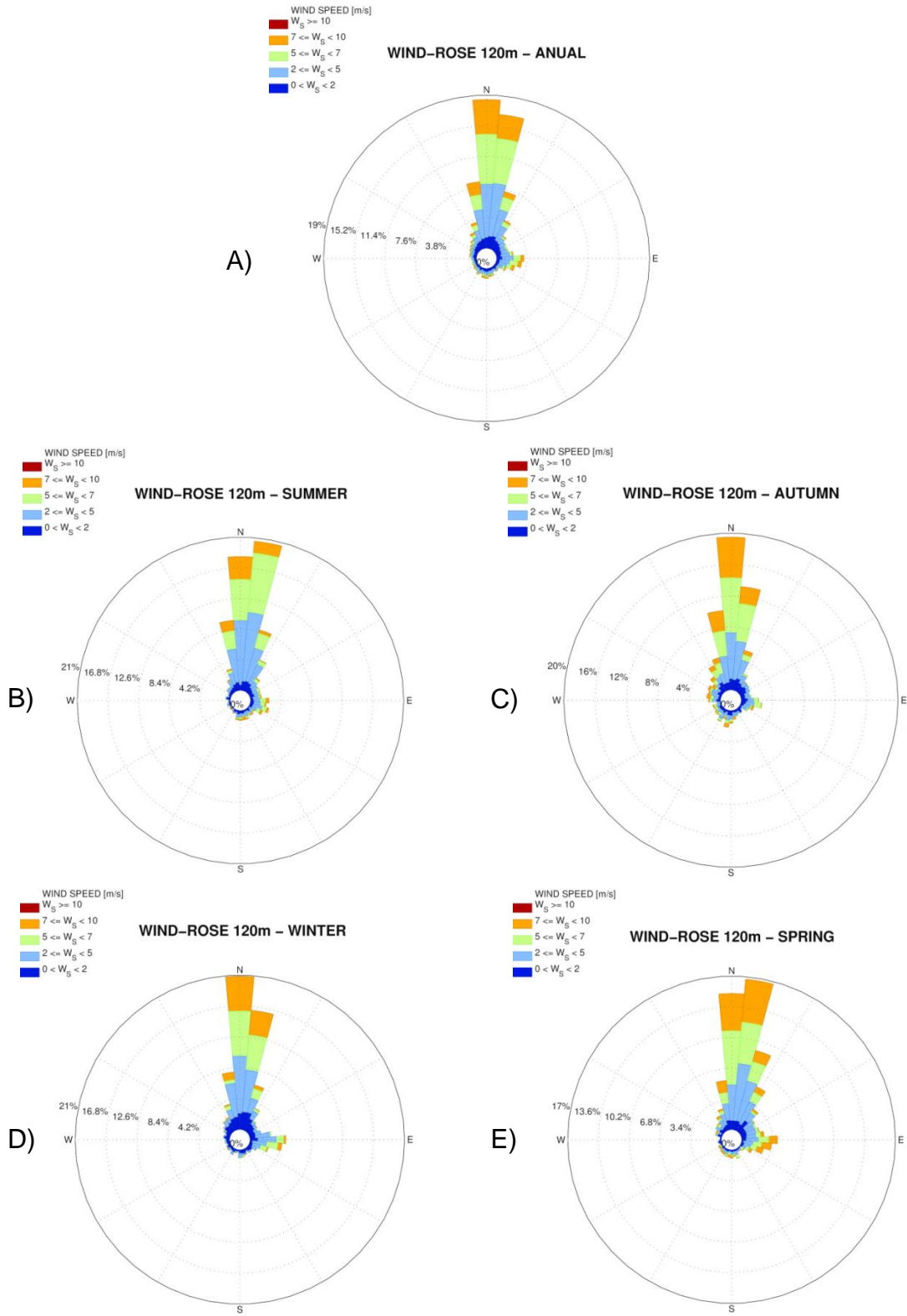
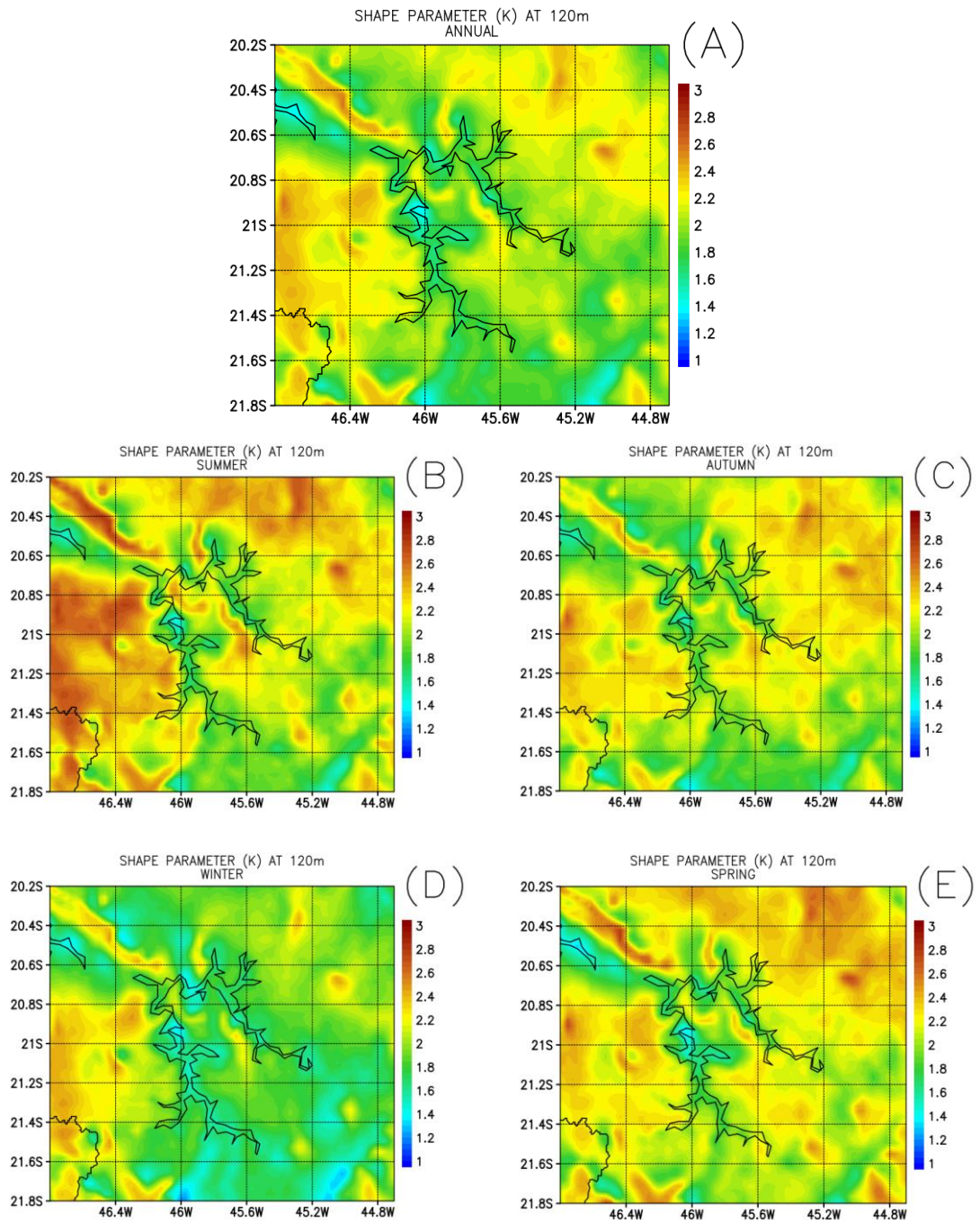**Figure 15**: Wind direction distribution from WRF at TILHA.

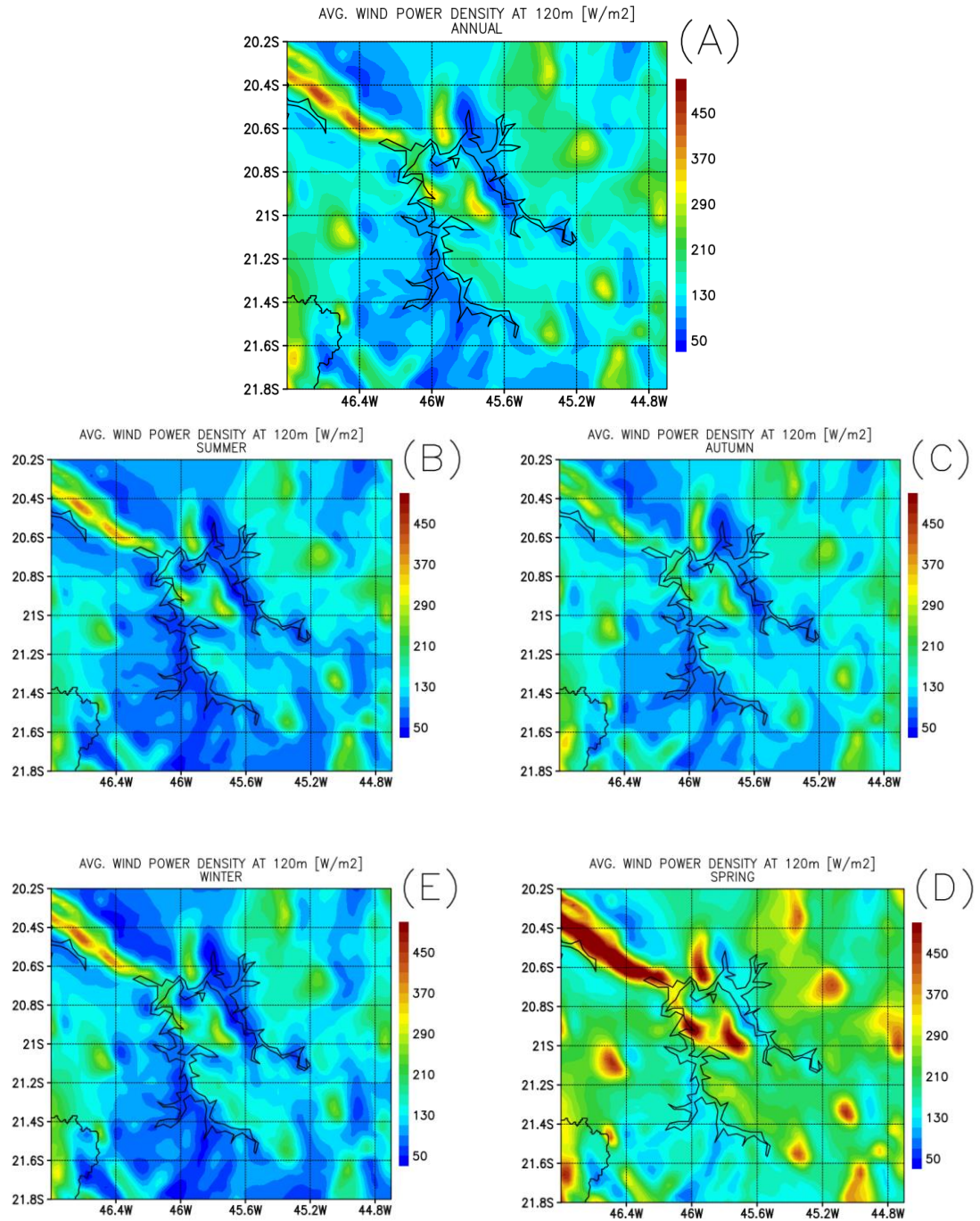**Figure 16**: Mean shape parameter, *k*, at 120 m based on the Weibull distribution. Seasonal and annual.

Figure 17: Average wind power density at 120 m. Seasonal and annual.
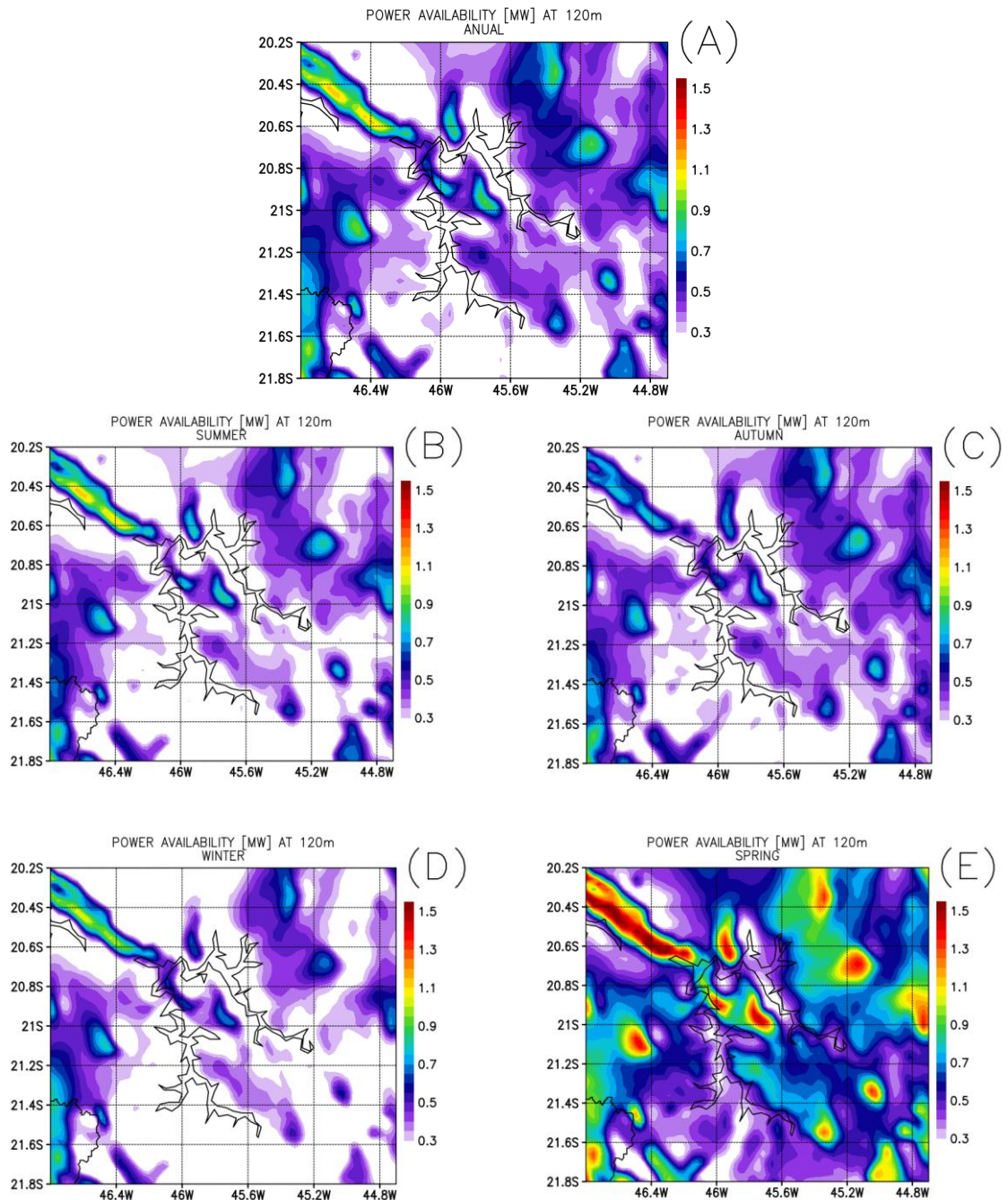
Figure 18: Wind power availability at 120 m. Seasonal and annual.

Figure 19 shows the percentage of wind power availability anomalies for the atmosphere under stable, neutral and unstable conditions, according to the Richardson Number. Results show a very clear pattern where the power production drops to almost 100% when the atmosphere is under stable conditions. During unstable events, the power production increases up to 120% (spring) with its lowest during the summer. The annual mean stays around 90% of increase. When the atmosphere is under neutral conditions, the production can increase up to 30%.

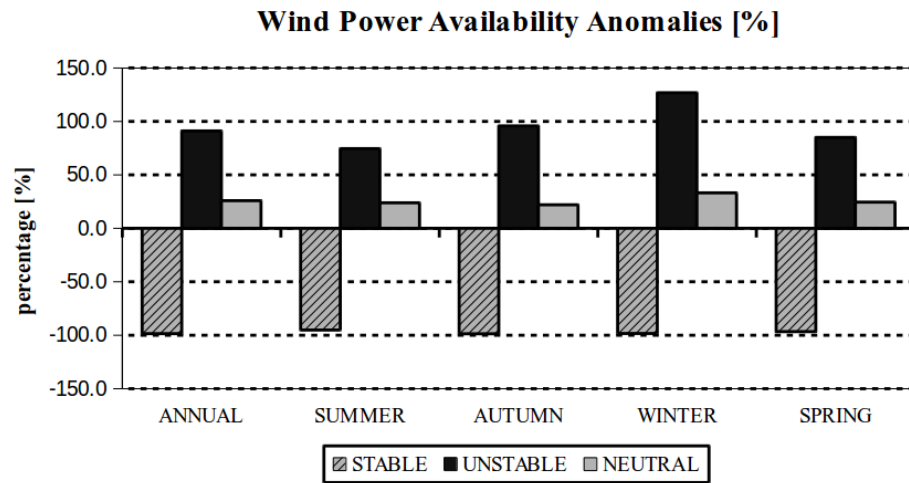**Figure 19**: Annual and seasonal percentage of wind power availability anomalies for the atmosphere under stable, neutral and unstable conditions.

4. CONCLUSIONS

The wind power assessment and production play an important role to diversify the energy matrix of a country. The dependence of an exclusive source is risky and does not make a nation prepared to possible natural disasters and periods of shortage. The lack of quality and frequent data makes its processes difficult and the numerical weather prediction can be a way to overcome such proposition.

The comparison between observed and modeled data presents satisfactory results when dealing with temperature, humidity and wind speed. The results at TILHA site were more promisors as well as the results for wind speed in T42M at 3 m. TTMR showed unsatisfactory results even for well-behaved variables such as TEMP. It can be an evidence of bad simulations or unrealistic/biased data recording in the instruments. Those patterns are strictly associated to the abrupt changes of roughness and energy balance between the station and its surroundings. The model was also able to recreate the wind speed distribution; however it showed some bigger discrepancies for T42M at 10 and 40 m.

In general, the comparisons for wind direction are satisfactory, excluding the ones from T42M at 20 m. For T42M the model did not show substantial differences about the wind direction for all vertical levels; however the observations were more dispersive.

The model outputs also show a better statistical fitting for punctual synoptic events, such as a cold front passing and a high pressure system, as presented. The amount of data and noise can imply in a less skilled statistic, mostly concerning the wind speed distribution and wind-roses within those short periods.

Finally, the assessment of wind power resources shows stronger winds during spring and well as a greater variance during the season. Furthermore, WRF presents a predominance of northerly winds for all seasons and the annual mean.

Both wind power density and wind power availability showed their maximum during spring, following the stronger winds during the season where this last one presents values up to 1.5 MW in the areas close to the mountains and their valleys.

Furthermore, the power production at TILHA is strongly affected by the stability profiles in the atmosphere. The production can drastically decrease in stable conditions and drastically increase during unstable events. In the end, we can conclude that the simulations performed represented an useful tool in order to assess the wind power resources over the Furnas reservoir. According to the model, the implementation of wind turbines (with a typical height around 120 m) can be more productive close to the mountains and inside the valleys.

The lake area seems to be less efficient to power production, except in the region surrounded by the division between its two branches.

This study can be an introduction to other researches also concerning the power production in water reservoirs. More specifically, it drives to studies about the power distribution, electric power network load, power demand, *smart grid* approaches, governmental actions, etc.

5. REFERENCES

AGÊNCIA BRASIL. **Setor de energia eólica vai investir R$ 15 bilhões em 2014**. Disponível em: <(http://agenciabrasil.ebc.com.br/pesquisa-e-inovacao/noticia/2014-08/setor-de-energia-eolica-vai-investir-r-15-bilhoes-em-2014)>. Acesso em: 4 de junho de 2015.

AHRENS, C. D. **Meteorology today: an introduction to weather, climate, and the environment**, 9th edn. Brooks/Cole Publications, 2000.

AMARANTE, O. A. C; BROWER, M.; ZACK, J.; DE SÁ, A. L. **Atlas do potencial eólico brasileiro**. Brasília: MME; Rio de Janeiro: Eletrobrás, 2001.

ANEEL – Agência Nacional de Energia Elétrica. **Energia Eólica**. Disponível em: <(http://www.aneel.gov.br/aplicacoes/atlas/pdf/06-energia_eolica%283%29.pdf)>. Acesso em: 4 de junho de 2015.

ASSIREU, A.T.; PELLEGRINI, C.C; PIMENTA, F.M. **Intensificação do vento devido a influências do relevo: evidências a partir de modelos numéricos e medidas *in situ***. Revista Ciência e Natura, v.X, p.60-62, 2013.

CARRILLO, C.; CIDRÁS, J.; DÍAZ-DORADO, E.; OBANDO-MONTAÑO, A.F. An Approach to Determine the Weibull Parameters for Wind Energy Analysis: The Case of Galicia (Spain). ***Energies*,** v. *7*, p. 2676-2700, 2014.

CHIN, H.N.S.; GLASCOE, L.; LUNDQUIST, J.; WHARTON, S. Impact of WRF Physics and Grid Resolution on Low-level Wind Prediction: Towards the Assessment of Climate Change Impact on Future Wind Power. In: Fifth International Symposium on Computational Wind Engineering (CWE2010), 2010, Chapel Hill, North Carolina, USA. **Anais do Fifth International Symposium on Computational Wind Engineering (CWE2010)**, Chapel Hill, USA.

DE CAMPOS, B.; ASSIREU, A.T.; CARVALHO, V.S.B. The atmospheric instability patterns in the planetary boundary layer related to different synoptic systems. In: **IX Micrometeorology Brazilian Workshop**, 2015, Santa Maria, Rio Grande do Sul, Brazil.

DE FOY, B.; ZAVALA, M.; BEI, N.; MOLINA, L. T. **Evaluation of WRF mesoscale simulations and particle trajectory analysis for the MILAGRO field campaign**. Atmos. Chem. Phys., v.9, p.4419-4438, 2009.

DEPPE, A.J.; GALLUS, W.A.; TAKLE, E.S. **A WRF Ensemble for Improved Wind Speed Forecasts at Turbine Height**. Wea. Forecasting, v.28, p.212–228.

DRAXL, C.; HAHMANN, A.N.; PENA, A.; NISSEN, J.N.; GIEBEL. G. **Validation of boundary-layer winds from WRF mesoscale forecasts with applications to wind energy**

forecasting. 19th Symposium on Boundary Layers and Turbulence. Keystone, CO, USA. Anais do 19th Symposium on Boundary Layers and Turbulence,   Keystone, USA.

FOKEN, T. 50 Years of the Monin–Obukhov Similarity Theory. **Boundary-Layer Meteorology**, v.119, n.3, p.431-447, 2006.

FOLEY, A.M.; LEAHY, P.G.; MARVUGLIA, A.; MCKEOGH, E.J. **Current methods and advances in forecasting of wind power generation**. Renewable Energy, v.37, n.1, p1-8, 2012.

GWEC.NET, (2015). **GLOBAL STATISTICS - GWEC**. [online] Available at: http://www.gwec.net/global-figures/graphs/ [Accessed 13 Aug. 2015].

GRUBB, M.J.; MEYER, N. I. Wind Energy: RESOURCE, Systems, and Regional Strategies. **Chapter 4 in Renewable Energy: Sources for Fuels and Electricity**, 1993.

HENNESSEY, J.P. Some aspects of wind power statistics. **J. Appl. Meteorol**., v. 16(2), p. 119–128, 1977.

HOLTON, J. **An introduction to dynamic meteorology**. Burlington, MA: Elsevier Academic Press, 2004.

JARVIS, A.; REUTER, H.I.; NELSON, A.; GUEVARA, E. **Hole-filled SRTM for the globe Version 4, available from the CGIAR-CSI SRTM 90m Database**, 2008. Disponível em: <http://srtm.csi.cgiar.org>. Acesso em: 18 de setembro de 2015.

KHANNA, S.; BRASSEUR, J.G. **Analysis of Monin–Obukhov similarity from large-eddy simulation**. Journal of Fluid Mechanics, v.345, p. 251-286, 1997.

LACKMANN, G. Midlatitude Synoptic Meteorology: Dynamics, Analysis, & Forecasting. **American Meteorological Society**, v.19, n.4, p.193–215.

LI, J.H.; GUO, Z.H.; WANG, H.J. Analysis of Wind Power Assessment Based on the WRF Model . **Atmos. Oceanic Sci. Lett.**, v.7, n.2, p.126-131, 2014.

MARIA, P.H.S.; COSTA, A.R.; SOMBRA, S.S. Modelagem numérica em alta resolução para previsão de geração de energia eólica no Ceará. **Rev. bras. meteorol.**, v.23, n.4, p.477-489, 2008.

MARTINS, F.R.; GUARNIERI, R.A.; PEREIRA, E.B. O aproveitamento da energia eólica. **Rev. Bras. Ensino Fís.**, v.30, n.1, p.1304.1-1304.13, 2008.

MATHWORKS INC., **MATLAB and Statistics Toolbox Release 2012b**. Natick, Massachusetts, United States, 2012.

MONIN, A.S.; OBUKHOV, A.M. Basic laws of turbulent mixing in the surface layer of the atmosphere. **Tr. Akad. Nauk SSSR Geofiz**. v.24, p.163–187.

MORGAN, E.C.; LACKNER, M.; VOGEL, R.M.; BAISE, L.G. Probability distributions for offshore wind speeds. **Energy Convers. Man.**, v.52, p.15–26, 2011.

NAWRI, N.; PETERSEN, G.N.; BJORNSSON, H.; HAHMANN, A.N.; JÓNASSON, K.; HASAGER, C.B.; CLAUSEN, N.E. The wind energy potential of Iceland. **Renewable Energy**, v.69, n.1, p.290-299, 2014.

NCEP – National Centers for Environmental Prediction/National Weather Service/NOAA/U.S. Department of Commerce.(2007). NCEP Global Forecast System (GFS) Analyses and Forecasts. **Research Data Archive at the National Center for Atmospheric Research, Computational and Information Systems Laboratory**. http://www.nco.ncep.noaa.gov/pmb/products/gfs/. Accesso em 1º de Fevereiro de 2015.

NREL.GOV, (2014). NREL: Wind Research - Wind Resource Assessment. [online] Available at: http://www.nrel.gov/wind/resource_assessment.html [Accessed 14 Aug. 2015].

PAHLOW, M.; PARLANGE, M.B.; PORTÉ-AGEL, F. On Monin-Obukhov Similarity In The Stable Atmospheric Boundary Layer. Boundary-Layer Meteorology, v.99, n.2, p. 225-248, 2001.

PIELKE, R.A. Mesoscale meteorological modeling. Second Edition. **International Geophysics Series**, v.78, n.1, p.676, 2002.

PORTAL FURNAS. **Furnas – Energia que impulsiona o Brasil**. Disponível em: <(http://www.furnas.com.br/frmEMQuemSomos.aspx)>. Acesso em: 4 de junho de 2015.

RAMOS, D.N.S.; LYRA, R.F.F.; SILVA JUNIOR, R.S. Previsão do vento utilizando o modelo atmosférico WRF para o estado de Alagoas**. Rev. bras. meteorol.**, v. 28, n.2, p.163-172, 2013.

RISØ-R-REPORT. **South Baltic Wind Atlas: South Baltic Offshore Wind Energy Regions Project**, 2011. Available at: <http://www.southbaltic-offshore.eu/reports-studies/img/SBO_Wind-Atlas.pdf>. Accessed on: 17th Oct 2015.

SHIMADA, S.; OHSAWA, T. Accuracy and characteristics of offshore wind speeds simulated by WRF. **Sola,** v.70, p.21–24, 2011.

SKAMAROCK, W.C. Evaluating Mesoscale NWP Models Using Kinetic Energy Spectra. Mon. **Wea. Rev.**, v.132, p.3019–3032, 2004.

SKAMAROCK, W.C.; KLEMP, J.B.; DUDHIA, J.; GILL, D.O.; BARKER, D.M.; DUDA, M.G.; HUANG, X.Y.; WANG, W.; POWERS, J.G. **A description of the Advanced Research WRF version 3**. NCAR Technical Note 475. Available at: <(http://www.mmm.ucar.edu/wrf/users/docs/arw_v3.pdf)>. Accessed on: 4th Jun 2015.

STULL, R. B. An introduction to boundary layer meteorology**. Dordrecht: Kluwer Academic**, p.666, 1988.

VALLE, R.M.; MOREIRA, G.A.A.; NASCIMENTO, C.A.M. Análise do potencial eólico de uma micro-região utilizando um modelo de camada limite atmosférica. **Revista Iberoamericana de Ingeniería Mecánica**, v.17, p.59-71, 2013.

WEIBULL, W. A statistical distribution function of wide applicability. **J. Appl. Mech.-Trans**. v. 18, n. 3, p. 293–297, 1951.

WILLMOTT, C.J. On the validation of models. **Physical Geography**, v. 2, p. 1984 – 194, 1981.

WINDUSTRY, (2015). Chapter 4: Wind Resource Assessment. [online] Available at: http://www.windustry.org/community_wind_toolbox-4-wind-resource-assessment [Accessed 14 Aug. 2015].

WISER, R.; YANG, Z.; HAND, M.; HOHMEYER, O.; INFIELD, D.; JENSEN, P.H.; NIKOLAEV, V.; O'MALLEY, M.; SINDEN, G.; ZERVOS, A. **Wind Energy. In IPCC Special Report on Renewable Energy Sources and Climate Change Mitigation**. Cambridge University Press, Cambridge, United Kingdom and New York, NY, USA, 2011.

WRF-MODEL.ORG, (2015). The Weather Research&Forecasting Model Website.. [online] Available at: http://www.wrf-model.org/index.php [Accessed 13 Aug. 2015].

WWEA – World Wind Energy Association. **WWEA publishes World Wind Resource Assessment Report 2014**. Disponível em: <(http://www.wwindea.org/wwea-publishes-world-wind-resource-assessment-report/)>. Acesso em: 4 junho 2015.